Available online at www.sciencedirect.com
ScienceDirect
International Journal of Heat and Mass Transfer 51 (2008) 1–12
International Journal of HEAT and MASS TRANSFER
www.elsevier.com/locate/ijhmt

Numerical simulations of nucleate boiling in impinging jets: Applications in power electronics cooling ☆

Sreekant Narumanchi [a,*], Andrey Troshko [b], Desikan Bharathan [a], Vahab Hassani [a]

[a] National Renewable Energy Laboratory, MS 1633, 1617 Cole Boulevard Golden, CO 80401-3393, USA
[b] ANSYS Inc., Fluid Business Unit, 10 Cavendish Court, Centerra Park Resource, Lebanon, NH 03766, USA

Received 25 October 2006; received in revised form 21 May 2007
Available online 15 August 2007

Abstract

Boiling jet impingement cooling is currently being explored to cool power electronics components. In hybrid vehicles, inverters are used for DC–AC conversion. These inverters involve a number of insulated-gate bipolar transistors (IGBTs), which are used as on/off switches. The heat dissipated in these transistors can result in heat fluxes of up to 200 W/cm^2, which makes the thermal management problem quite important.

In this paper, turbulent jet impingement involving nucleate boiling is explored numerically. The framework for these computations is the CFD code FLUENT. For nucleate boiling, the Eulerian multiphase model is used. The numerical results for boiling water and R113 jets (submerged) are validated against existing experimental data in the literature. Some representative IGBT package simulations that use R134a as the cooling fluid are also presented.

Keywords: Boiling; Power electronics; Numerical simulations; CFD; IGBTs

1. Introduction

Significant attention has been devoted to electronics cooling studies over the past two decades. In this context, single-phase liquid jets have been studied very extensively in the literature [1–4]. These studies include experiments, theoretical analyses, and numerical simulations. Considerable attention has also been focused on boiling jets. Boiling liquid jets take advantage of the latent heat of vaporization of the fluid to provide fairly high-heat transfer coefficients (>20,000 W/m^2 K), which makes them attractive for electronic cooling applications. The boiling curve for a saturated liquid is shown in Fig. 1.

Typically, for electronic cooling applications involving two-phase flow, nucleate boiling is the preferred regime of operation because a small increase in wall superheat is accompanied by a large increase in the wall heat flux. Also, in electronics, it may not be possible to afford very large temperature differences between the solid surfaces and the liquid—a characteristic essential for regimes such as film boiling.

A number of studies have been carried out to enhance heat removal from electronic packages (e.g. [5–7]).

In the context of boiling liquid jets, extensive work has already been reported in the literature [8–12]. Many studies have been carried out with circular [13–20] as well as planar [21–24] jets in both free-surface and submerged configurations. This includes single and multiple jets [17,25–29].

In the nucleate boiling literature, most of the correlations are cited in the following form:

* Corresponding author. Tel.: +1 303 275 4062; fax: +1 303 275 4415.
E-mail address: sreekant_narumanchi@nrel.gov (S. Narumanchi).

0017-9310/$ - see front matter © 2007 Elsevier Ltd. All rights reserved.
doi:10.1016/j.ijheatmasstransfer.2007.05.026

Nomenclature

$C_{\varepsilon 1}, C_{\varepsilon 2}$	constants
C_P	specific heat (J/kg K)
d	jet diameter (m)
D	target equivalent diameter (m)
f	bubble departure frequency (Hz)
$\vec{F}$	force vector (N/m)
$\vec{g}$	gravitational acceleration vector (m/s^2)
G	term in the turbulent kinetic energy equation (kg/m s^3)
h	heat transfer coefficient (W/m^2 K)
IGBT	insulated-gate bipolar transistor
k	thermal conductivity (W/m K)
k	turbulence kinetic energy (m^2/s^2)
L	latent heat (J/kg)
$\dot{m}$	mass transfer (kg/m^3 s)
n	nucleation site density
p	pressure (N/m^2)
Pr	Prandtl number
q, q''	heat flux (W/m^2)
$\vec{q}$	heat flux vector (W/m^2)
Q	interfacial energy exchange (W/m^3)
$\vec{R}$	interfacial drag force (N/m^3)
Re	Reynolds number
S	source term in energy equation (W/m^3)
S_k	source term in turbulent kinetic energy equation (kg/m s^3)
S_ε	source term in dissipation rate equation (kg/m s^4)
u, U	liquid velocity (m/s)
v	phase velocity (m/s), jet velocity at the nozzle exit (m/s)
$\vec{v}$	velocity vector (m/s)

Greek symbols

α	phase volume fraction
ΔT	temperature difference (K)
ε	dissipation rate (m^2/s^3)
η	thermal diffusivity (m^2/s)
κ	thermal conductivity (W/m K)
μ	dynamic viscosity (Ns/m^2)
ν	kinematic viscosity (m^2/s)
ρ	density (kg/m^3)
σ	surface tension (N/m)
$\bar{\bar{\tau}}$	shear stress (N/m^2)

Subscripts

avg	average
CHF	corresponding to critical heat flux
d	jet diameter
eff	effective
f	corresponding to fluid
l	corresponding to liquid
lv	corresponding to interaction between liquid and vapor
pq	corresponding to interaction between phases p and q
q	corresponding to phase q
sat	corresponding to saturation
sub	corresponding to sub-cooling
v	corresponding to vapor
vw	vapor and close to the wall

Superscript

cell	cell value

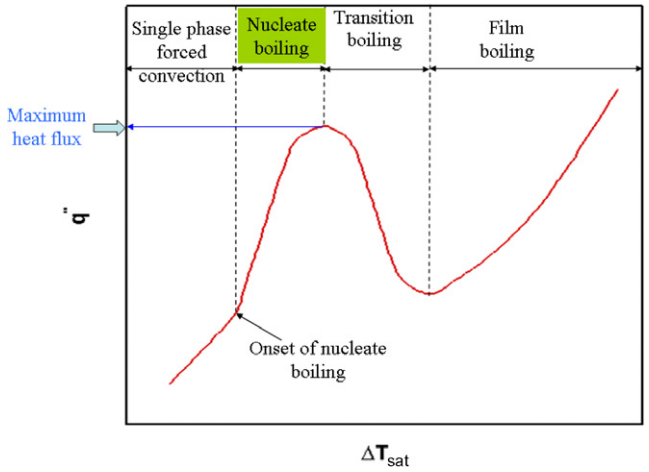

Fig. 1. General boiling curve for saturated liquids.

$$q'' = C\Delta T_{sat}^{m} \tag{1}$$

where C and m are determined by curve fit to the experimental data, $\Delta T_{sat} = T_{wall} - T_{sat}$ is the wall superheat, T_{sat} is the saturation temperature of the fluid, T_{wall} is the wall temperature, and q'' is the wall flux. Most of the heat transfer data are cited in the form given in Eq. (1), which can be rewritten as:

$$h = \frac{q''}{\Delta T_{sub} + \left(\frac{q''}{C}\right)^{1/m}} \tag{2}$$

where h is the heat transfer coefficient, $\Delta T_{sub} = T_{sat} - T_f$ is the fluid sub-cooling and T_f is the ambient fluid temperature.

Nucleate boiling is governed by intense bubble nucleation and mixing, so it does not depend on many jet parameters, unlike single-phase jets. Jet diameter, jet orientation, number of jets, jet configuration (free-surface or submerged), and even jet velocity do not have much effect on the heat transfer in the nucleate boiling regime [8].

The target surface plays a critical role in the bubble nucleation process [30]. In fact, much of the difficulty in obtaining truly non-dimensional correlations for nucleate boiling arises from this. Surface conditions, surface aging,

and even the condition of the surface during the course of an experiment [13] all may have a considerable impact on the heat transfer results.

The other aspect that has been given considerable attention is the critical heat flux (CHF) (Fig. 1) [8,11]. When CHF occurs, the temperature of the wall suddenly increases because of dry-out conditions in which no liquid is in contact with the surface to sustain boiling. A schematic of this phenomenon is shown in Fig. 2 [8]. The liquid sub-layer drawn from the main liquid jet supply sustains the boiling process. When liquid cannot be supplied to this sub-layer, dry-out occurs, and CHF is reached.

Considerable work has been done to develop non-dimensional correlations that show the dependence of the CHF on other parameters [16,28,31–35]. Typically, empirical correlations are presented only for certain simple geometries. For thermal design that involves more complicated geometries, it is important to have CFD modeling capability. Some multiphase models have been presented in the literature [36,37] and modeling of nucleate boiling on a surface has been attempted [38]. However, CFD modeling of boiling jets is still in its infancy [39,40]. Numerical studies of phenomena such as nucleate pool boiling [41,42] and film boiling [43–45] are just beginning to appear in the literature.

A significant amount of experimental work has also been reported in the literature on spray cooling (e.g. [46–48]). Both sprays and jets have their advantages and disadvantages. For some applications, sprays might be more suitable, while for others, jets may be a better choice.

This paper presents CFD modeling of jets involving nucleate boiling. The overall effort in this area falls under the general program for thermal control of the Department of Energy's Advanced Power Electronics and Electrical Machines (APEEM) program. The National Renewable Energy Laboratory (NREL) leads research and development activities in thermal control related to the APEEM program. The broad FreedomCAR goal is to dissipate 200–250 W/cm^2 heat flux from the silicon die while keeping the die temperature below 125 °C. The overall objective of the thermal control activities is to develop advanced technologies and effective integrated thermal control systems, aimed to meet the FreedomCAR program goals. The FreedomCAR goals address key requirements for power electronics such as target values for volumes, cost and weight of various subcomponents. The barriers for thermal control technologies are affected by the overall specifications related to these quantities.

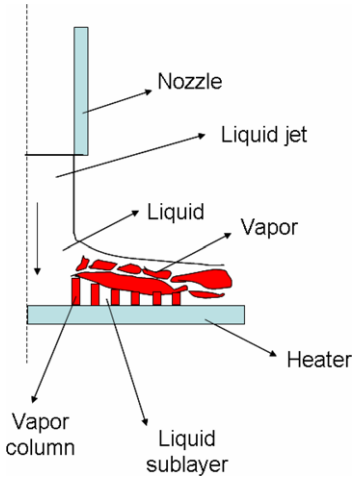

Fig. 2. Mechanism by which critical heat flux occurs.

For nucleate boiling, the Eulerian multiphase model is used. A mechanistic model of nucleate boiling is implemented in a user-defined function (UDF) in FLUENT. The numerical predictions are validated against experimental studies on submerged jets involving nucleate boiling. These experimental studies involve water and R-113 as the fluids. IGBT package simulations are also reported with a submerged boiling jet of R134a.

To the best of our knowledge, these validations and IGBT package simulations with boiling jets are being reported for the first time. A comparison between single-phase and boiling jets from the heat transfer viewpoint and in the context of cooling the IGBT package is also presented.

2. CFD modeling of jets in the nucleate boiling regime: model description

In this section, we present a CFD model of nucleate boiling. The model is described below.

2.1. Eulerian multiphase model description

The following are equations for the conservation of mass, momentum, and energy.

Mass conservation equation for phase q:

$$\frac{\partial}{\partial t}(\alpha_q\rho_q) + \nabla\cdot(\alpha_q\rho_q\vec{v}_q) = \sum_{p=1}^{n}\dot{m}_{pq} \tag{3}$$

where α is the phase volume fraction of phase q, ρ is the density, $\vec{v}$ is the velocity vector, and $\dot{m}$ is the volumetric mass exchange rate between phases p and q.

Momentum conservation equation for phase q:

$$\begin{aligned}\frac{\partial}{\partial t}(\alpha_q\rho_q\vec{v}_q) &+ \nabla\cdot(\alpha_q\rho_q\vec{v}_q\vec{v}_q)\\ &= -\alpha_q\nabla p + \nabla\cdot\bar{\bar{\tau}}_q + \alpha_q\rho_q\vec{g}_q + \sum_{p=1}^{n}(\vec{R}_{pq} + \dot{m}_{pq}\vec{v}_{pq})\\ &\quad + \alpha_q\rho_q(\vec{F}_q + \vec{F}_{\text{lift},q} + \vec{F}_{vm,q})\end{aligned} \tag{4}$$

where $\bar{\bar{\tau}}$ is the shear stress, $\vec{R}$ is the interfacial drag force, $\vec{F}_q$ is the turbulent diffusion force, $\vec{F}_{\text{lift},q}$ is the lift-force, p is the pressure, and $\vec{g}$ is the gravitational acceleration vector.

Energy conservation equation for phase q:

$$\begin{aligned}\frac{\partial}{\partial t}(\alpha_q\rho_q h_q) &+ \nabla\cdot(\alpha_q\rho_q\vec{v}_q h_q)\\ &= -\alpha_q\frac{\partial p}{\partial t} + \bar{\bar{\tau}}_q : \nabla\vec{v}_q - \nabla\vec{q}_q + S_q + \sum_{p=1}^{n}(Q_{pq} + \dot{m}_{pq}h_{pq})\end{aligned} \tag{5}$$

where h is the enthalpy, $\vec{q}$ is the heat flux vector, S is the source term, Q is the energy exchange term between the different phases, and h_{pq} is the difference in the formation enthalpies of phases p and q.

The following are restrictions on interfacial mass, momentum, and energy interfacial exchange terms:

$$\dot{m}_{pq} = -\dot{m}_{qp}, \quad \dot{m}_{pp} = 0 \tag{6}$$

$$\vec{R}_{pq} = -\vec{R}_{qp}, \quad \vec{R}_{pp} = 0 \tag{7}$$

$$Q_{pq} = -Q_{qp}, \quad Q_{pp} = 0 \tag{8}$$

Most sub-cooled boiling flows are turbulent, so the mixture phase k-epsilon model is used:

$$\frac{\partial}{\partial t}(\rho_m k) + \nabla \cdot (\rho_m \vec{v}_m k) = -\nabla \cdot \left(\frac{\mu_{t,m}}{Pr_k}\nabla k\right) + G_{k,m} - \rho_m \varepsilon + S_k \tag{9}$$

where k is the turbulent kinetic energy, μ is the viscosity, ε is the dissipation rate, G is the turbulence production rate, and S is the bubble-induced turbulence in the turbulent kinetic energy equation

$$\frac{\partial}{\partial t}(\rho_m \varepsilon) + \nabla \cdot (\rho_m \vec{v}_m \varepsilon) = -\nabla \cdot \left(\frac{\mu_{t,m}}{Pr_\varepsilon}\nabla \varepsilon\right) + \frac{\varepsilon}{k}(C_{\varepsilon 1} G_{k,m} - C_{\varepsilon 2}\rho_m \varepsilon) + S_\varepsilon \tag{10}$$

where $C_{\varepsilon 1}$, $C_{\varepsilon 2}$ are constants and S_ε is the bubble-induced dissipation in the dissipation rate equation.

What follows is a closure for interfacial terms in the sub-cooled boiling model.

2.2. Mass conservation equation

Rate of vapor formation per unit of volume in Eq. (3) becomes:

$$\sum_{p=1}^{n} \dot{m}_{qp} = \dot{m}_{lv} = [h_{ls}(T_l - T_s) + h_{vs}(T_v - T_s)]A_i/L + q''_E A_w/(L + C_{pl}(T_S - T_L)) \tag{11}$$

where h_{ls} is the liquid side interfacial heat transfer coefficient calculated from the Ranz-Marshall correlation;

$$A_i = 6\alpha_{sv}(1 - \alpha_v)/d_v \tag{12}$$

is the interfacial area density, where $\alpha_{sv} = \min(\alpha_v, 0.25)$ (Kurul and Podowski [36]); $h_{vs} = 10^5$ W/m^2/K is the vapor side interfacial heat transfer coefficient – its large value stems from the assumption that vapor temperature is close to saturation, i.e., interface temperature; q''_E is the evaporative heat flux calculated from the RPI model [36,37]; $L = h^0_{vs} - h^0_{ls}$ is the latent heat per unit mass; $A_w = \delta(\vec{x} - \vec{x}_w)$ is interfacial area density of wall surface; and d_v is the diameter of the secondary phase (vapor bubble). Here, subscripts l, v, and s mean liquid phase, vapor phase, and saturation state, respectively. In discretized form, A_w becomes the ratio of the cell face area constituting the wall to the volume of the cell next to this face. Eq. (11) implies that boiling occurs when heat is added to the interface and condensation occurs when heat is removed from the interface.

2.3. Momentum conservation equation

The interfacial drag force per unit volume is calculated as:

$$\vec{R}_{lv} = 0.75 \cdot C_d \cdot \rho_l \cdot \alpha_v \cdot |\vec{v}_r| \cdot \vec{v}_r/d_v \tag{13}$$

where the drag coefficient C_d is calculated as:

$$C_d = \mathrm{MIN}(C_d^{dis}, C_d^{vis}) \tag{14}$$

where C_d^{dis} and C_d^{vis} are known drag correlations calculated for distorted and viscous regimes accounting for the high concentration effect:

$$C_d^{vis} = \frac{24}{Re_b}(1 + 0.1Re_b^{0.75}) \cdot (\mathrm{MAX}(\alpha_l, 0.5))^{-2} \tag{15}$$

$$C_d^{dis} = \frac{2d_v}{3}(g(\rho_l - \rho_v)/\sigma)^{1/2} \cdot (\mathrm{MAX}(\alpha_l, 0.5))^{-1} \tag{16}$$

The lift-force coefficient is calculated as (Moraga et al. [49]):

$$C_l = \begin{cases} 0.0767, & \phi \leqslant 6000 \\ -(0.12 - 0.2e^{-\phi/36000})e^{\phi/3e+07}, & 6000 < \phi < 1.9e+05 \\ -0.002, & \phi \geqslant 1.9e+05 \end{cases} \tag{17}$$

where $\phi = Re_b Re_v$. This lift coefficient combines the opposing actions of two lift-forces. "Classical" aerodynamics lift-force results from interaction between bubble and liquid shear, and lateral force results from interaction between bubbles and vortices shed by bubble wake. Here, $Re_b = d_v|\vec{v}_r|/\nu_l$ is the bubble Re, and $Re_v = d_v^2|\nabla \times \vec{v}_l|/\nu_l$ is the bubble shear Re.

Turbulent diffusion force is calculated as [36]:

$$\vec{F}_v = -\vec{F}_l = -C_{TD}\rho_l k \nabla \alpha_v \tag{18}$$

where turbulent dispersion coefficient $C_{TD} = 1.0$ was used.

2.4. Energy conservation equation

The wall superheat is a source of vapor bubbles reflected in Eq. (3). In general, the energy balance at the infinitely thin wall separating fluid and solid cells is:

$$h_{sol,w} \cdot (T_{sol}^{cell} - T_w) = \alpha_l^{cell}[q''_E + q''_Q + q''_l] + \alpha_v^{cell}[h_{vw} \cdot (T_w - T_v^{cell})] \tag{19}$$

where the left-hand side of Eq. (19) is solid side heat flux due to conduction, the first and second terms on the right-hand side of Eq. (19) denote parts of heat flux going into liquid and vapor phases, respectively.

According to the RPI model, part of the total heat flux from wall to liquid phase is partitioned into three components:

$$q''_w = q''_l + q''_Q + q''_E \tag{20}$$

which are liquid convective heat flux, quenching heat flux, and evaporative heat flux, respectively. Under sub-cooled boiling conditions, the wall surface is subdivided into portion Ω ($0 \leqslant \Omega \leqslant 1$), covered by nucleating bubbles, and portion $1-\Omega$, covered by fluid. Therefore, convective heat flux is expressed as:

$$q''_l = h_{lw} \cdot (T_w - T_l^{cell}) \cdot (1-\Omega) \tag{21}$$

where h_{lw}, the single-phase heat transfer coefficient, is derived from either log law if flow is turbulent or Fourier law if flow is laminar. Liquid phase properties must be used while calculating h_{lw} for either turbulent or laminar flow.

Quenching heat flux q''_Q models additional energy transfer related to liquid filling the wall vicinity after the bubble detachment:

$$q''_Q = 2\pi^{-0.5}\Omega(f\kappa_l\rho_l C_{pl})^{0.5}(T_w - T_l^{cell}) \tag{22}$$

where f is the bubble departure frequency, κ is the thermal conductivity, C is the specific heat, and ρ is the density.

Evaporative heat flux is given by:

$$q''_E = \frac{\pi}{6} d_{vw}^3 f n \rho_v L \tag{23}$$

where d_{vw} is the bubble departure diameter, and n is the nucleation site density.

In Eqs. (21)–(23), closure must be provided for wall boiling parameters. Correct prediction of bubble departure diameter d_{vw} is very important because evaporation heat rate depends strongly on this parameter, according to Eq. (23). At saturated boiling, the departure diameter is controlled mainly by forces acting on growing bubble at the wall, in sub-cooled boiling this value is controlled by condensation at the top of the bubble. An expression for sub-cooled controlled d_{vw} was provided by Unal [50] and Wei and Morel [51]. In this paper, we will simulate saturated boiling. Zeng [52] considered a growing bubble at the wall as an ellipsoid with the major axis located at a certain angle with respect to the wall normal. After reaching a certain diameter called departure diameter, bubble does not leave the wall but slides along it and, finally, leaves the wall with a diameter called lift-off diameter. All this movement happens under various forces acting on bubble – acceleration, gravity, drag, lift and, at very high wall superheat, additional drag caused by neighbor bubbles (Kolev [53]). Rigorous accounting of all these forces would lead to a system of two transcendental equations (force balance in two directions – parallel and normal to wall), which is computationally expensive. Instead, making two simplifying assumptions allows analytical expression from force balance. First, it is assumed that the bubble departure diameter and bubble lift-off diameter are nearly equal in the absence of liquid shear, i.e., for pool boiling (Kolev [53]). Second, Zeng [52] assumed that since lift-off diameter does not depend on liquid shear, this diameter is controlled by only two wall normal forces – gravity and acceleration at the moment of lift-off. Acceleration force is calculated from the assumption that bubble growth at the superheated wall is diffusion controlled so the bubble diameter varies as (Koumoutsos [54]):

$$d_{vw} = \pi^{-1/2}\left(\frac{\rho_l C_{pl}(T_w - T_s)}{\rho_v L}\right)(\eta t)^{1/2} \tag{24}$$

where η is the thermal diffusivity.

The expression for acceleration force acting on the bubble is [53]:

$$F_{ac} = \frac{\rho_l \pi d_{vw}}{8}\left(\frac{3}{2}\dot{d}_{vw}^2 + d_{vw}\ddot{d}_{vw}\right) \tag{25}$$

and gravity force acting on the bubble is:

$$F_{grav} = \frac{4(\rho_l - \rho_v)\pi d_{vw}^3 g}{3} \tag{26}$$

Equating forces in Eqs. (25) and (26) and using Eq. (24) for time derivatives leads to the following expression for bubble departure diameter in the absence of liquid shear (pool boiling):

$$d_{vw} = 3\left[\frac{\rho_l}{2(\rho_l - \rho_v)g}\left(\frac{\rho_l C_{pl}(T_w - T_s)\eta^{1/2}}{\rho_v L}\right)^4\right]^{1/3} \tag{27}$$

Comparison of Eq. (27) with experimental pool-boiling data at atmospheric pressure and prediction of Kolev model [53] is displayed in Fig. 3.

As shown, the model equation tends to overpredict data and Kolev's calculations at higher superheats. This is expected since Kolev's calculations include all forces. In particular, Kolev's equation includes liquid shear drag that becomes important for larger bubbles at higher superheats and tends to reduce bubble departure diameter. However, overall, Eq. (27) is deemed to produce reasonable agreement with experimental data. Fig. 4 depicts dependence of d_{vw} with pressure for pool boiling at fixed superheat.

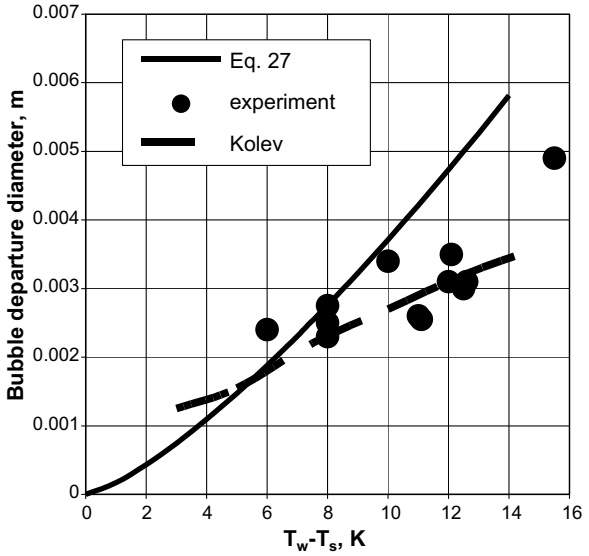

Fig. 3. Comparison of Eq. (27) to pool-boiling experimental data and calculations of Kolev [53].

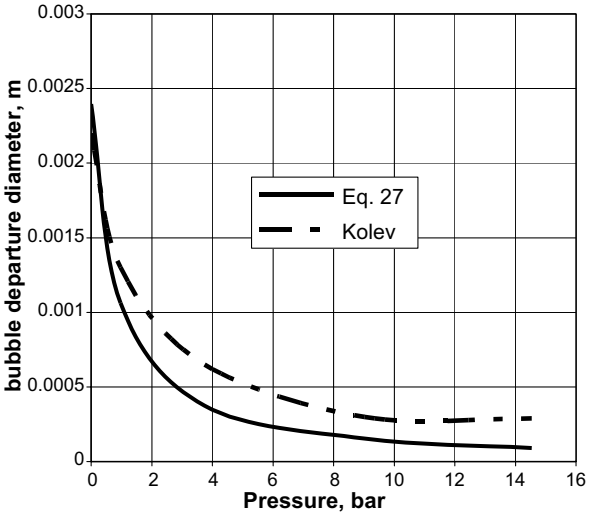

Fig. 4. Comparison of Eq. (27) to the calculations of Kolev.

A comparison is shown with the calculations of Kolev [53] which were very close to experimental data. As shown, it correctly predicts the trend of bubble size reduction with increasing pressure, but the magnitude of this reduction is overpredicted. Therefore, an empirical pressure correction multiplier to the r.h.s of Eq. (27) was introduced in the form $f_1 = 1 + 0.1503 \cdot (p \times 10^{-5} - 1.01352)$, where p is the pressure in Pascal.

As mentioned before, Eq. (27) predicts lift-off bubble diameter which is almost equal to departure diameter for pool boiling. For forced convection boiling, liquid shear induces additional drag force on the bubble and effectively reduces d_{vw}. Data of Koumoutsos [54] was used to deduce correction multiplier which takes liquid velocity in the near wall cell as an argument to calculate the multiplier in the form $f_2 = \exp(-6.3512 \cdot |\vec{u}_l|)$. Therefore, the final expression for bubble departure diameter used in the present model is

$$d_{vw} = 3 \cdot f_1 f_2 \cdot \left[\frac{\rho_l}{2(\rho_l - \rho_v)g} \left(\frac{\rho_l C_{pl} (T_w - T_s) \eta^{1/2}}{\rho_v L} \right)^4 \right]^{1/3} \tag{28}$$

Eq. (28) is deemed to be a good compromise between simplicity and accuracy. It reproduces correctly all important trends for pool and convective boiling. However, it should not be used for very high wall superheats above 20 K, when nucleate boiling is still taking place, as neighbor bubble-induced drag important in this region is not accounted for.

Nucleation site density is given by the following relation (Podowski et al. [37]):

$$n = (200(T_w - T_{sat}))^{1.80} \tag{29}$$

Bubble departure frequency is calculated as:

$$f = \sqrt{\left(\frac{4g(\rho_l - \rho_v)}{3 d_{vw} \rho_l} \right)} \tag{30}$$

The effective wall area occupied by boiling sites is given by:

$$\Omega = \min(0.25 \cdot \pi d_{vw}^2 n \eta, 1.0) \tag{31}$$

where $\eta = 4.8 \cdot \exp(-Ja/80)$, and Jacob number is given by (Kenning and Victor [55]) $Ja = C_{pl} \cdot \rho_l (T_s - T_l) \cdot (\rho_v L)^{-1}$.

Bubble diameter in free stream is given by either a constant value or by Unal's correlation as a function of local sub-cooling $T_{sub} = T_{sat} - T_l$ (Kurul and Podowski [36]):

$$d_v = \begin{cases} 1.5 \times 10^{-4}, & T_{sub} > 13.5 \text{ K} \\ 1.5 \times 10^{-3} - 10^{-4} \times T_{sub}, & 0 < T_{sub} < 13.5 \text{ K} \\ 1.5 \times 10^{-3}, & T_{sub} < 0 \end{cases} \tag{32}$$

2.5. Turbulence equations

The conventional mixture k-epsilon model contains two additional terms that describe additional bubble stirring and dissipation: one in turbulent kinetic energy and one in dissipation rate equation:

$$S_k = 0.75 \cdot C_d \cdot \rho_l \cdot \alpha_v \cdot |\vec{v}_r|^2 / d_v \tag{33}$$

$$S_\varepsilon = C_{\varepsilon 3} \frac{3 C_d |\vec{v}_r|}{d_v} S_k \tag{34}$$

where $C_{\varepsilon 3} = 0.45$ (Troshko and Hassan [56]).

3. Experimental validations

In this section, we present validation of the code with some experimental results with submerged jets involving nucleate boiling.

3.1. Comparison with experimental study of Katto and Kunihiro [14]

First, we examine the experimental study of Katto and Kunihiro [14]. The domain and boundary conditions are shown in Fig. 7. A water jet with 3 °C sub-cooling at atmospheric pressure (i.e., with $T_{inlet} = 97$ °C) impinges on a 10-mm-diameter disk with an inlet velocity of 2 m/s. The baseline nozzle diameter is 1.6 mm, and the distance between the nozzle exit and the heated plate is maintained at 3 mm. A heat flux is imposed on the hotplate surface, as shown in Fig. 5. This is a submerged jet configuration. An axisymmetric domain is established. The RNG k-epsilon model with standard wall functions is used. With the use of the standard wall function, the $y+$ close to the walls should be maintained above 30.

All the results presented here are mesh-independent to within 5%. The properties of water at 1 atmosphere pressure are listed in Table 1.

There is ambiguity about the wall temperature measured in the experiments. All indications are that the stagnation point temperature is reported in the experiments. Fig. 6 shows the boiling curve – which is a plot of the wall heat flux vs. the stagnation point wall superheat. The wall superheat is defined as $\Delta T_{sat} = T_w - T_{sat}$, where T_w is the wall

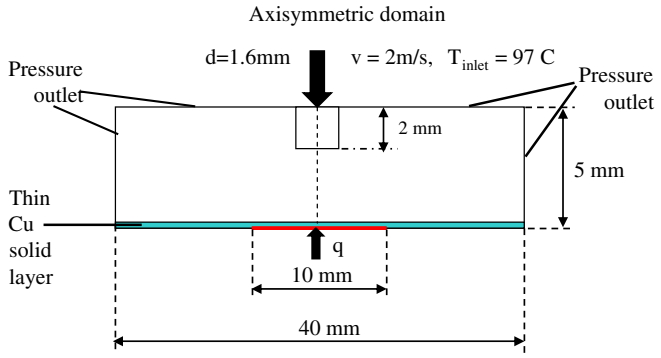

Fig. 5. Axisymmetric domain used for the Katto and Kunihiro study (1973) with submerged water jets involving nucleate boiling.

Table 1
Properties of water and R-113 at 1 atmospheric pressure (1.013$e+05$ Pa)

	Water		R-113	
	Liquid	Vapor	Liquid	Vapor
Saturation temperature (°C)	100		47.6	
Surface tension (N/m)	0.059		0.014	
Latent heat (J/kg)	2,257,000		144,000	
Density (kg/m^3)	958	0.6	1507	7.5
Specific heat (J/kg K)	4219	2010	980	724
Dynamic viscosity (N s/m^2)	2.83e−04	1.23e−05	5.23e−04	1.08e−05
Thermal conductivity (W/m K)	0.68	0.025	0.074	0.01

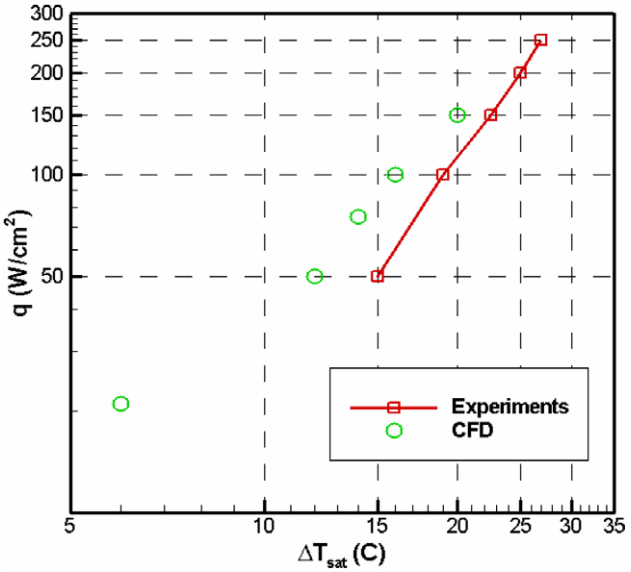

Fig. 6. Boiling curve for the Katto and Kunihiro (1973) [14] study.

stagnation point temperature while T_{sat} is the saturation temperature of the fluid at the inlet pressure. The experimental data are close to the stagnation superheat (within 20%), which is encouraging. Given the nature of this problem, uncertainties on the order of even 30% are acceptable. There is temporal fluctuation in all quantities—such as temperature, fluid volume fraction, mass flow rates, and energy transfer rates—obtained from the CFD simulations. A temporal average is reported here.

It has also been reported in the literature [8,14,16] that the nucleate boiling phenomena is independent of the jet orientation as well as the jet diameter. We were able to capture this in the numerical simulations too – though results are not reported here.

3.2. Comparison with experimental results of Zhou and Ma [9]

In this section, we consider another experimental study with submerged boiling jets. This is the study by Zhou and Ma [9] with a submerged R-113 jet. The rationale for choosing this study is because it involves a fluid other than water, it involves sub-cooling and is performed at both low (0.41 m/s) and high (11.36 m/s) velocities. The domain is shown in Fig. 7. As a simplification, the domain is assumed to be axisymmetric. The nozzle diameter is 1 mm. The target plate (constantan foil) area in the actual experiment is 5 mm × 5 mm, corresponding to a disk of radius 2.8 mm. A heat flux is applied to the target surface. The distance between the end of the nozzle and the target surface is 5 mm. In the experiments, the stagnation zone temperature is measured with a spatial resolution of about 0.2 mm. Also, the direction of gravity is not the same as in the actual experiment. However, we have confirmed through simulations that the impact of gravity on nucleate boiling in impinging jets is not important. This aspect has also been demonstrated experimentally, as mentioned previously.

The boiling curves (heat flux vs. stagnation point wall superheat) from both experiments and the CFD predictions are plotted in Fig. 8. Fig. 8a shows the curve for a jet velocity of 0.41 m/s while Fig. 8b for jet velocity of 11.36 m/s. The R-113 properties at atmospheric pressure are listed in Table 1. The fluid sub-cooling is 18.5 °C, which means that the jet inlet temperature is 302.3 K. Two different jet velocities are presented: 0.41 and 11.36 m/s. At the elevated velocity, the saturation temperature of the fluid

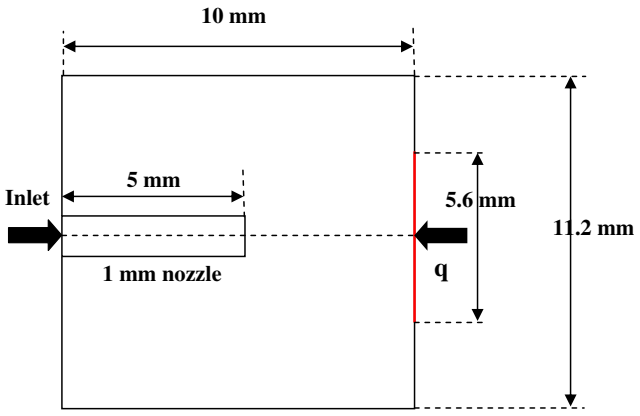

Fig. 7. Domain for the Zhou and Ma (2004) study with submerged jets of R113 involving nucleate boiling.

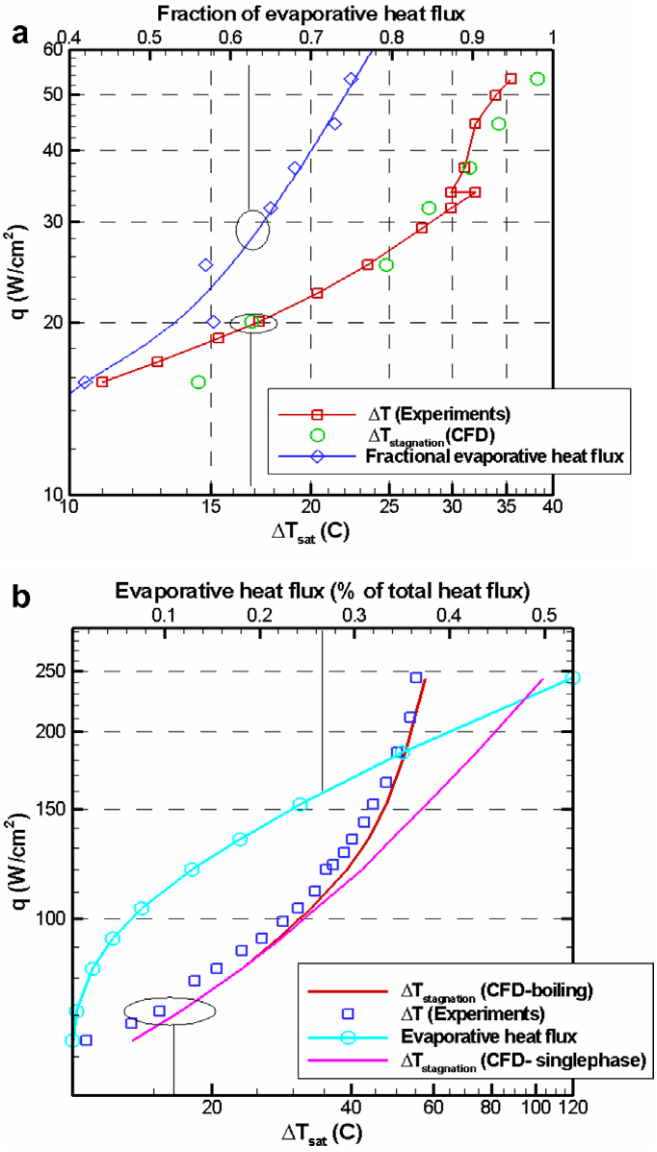

Fig. 8. Boiling curve at different velocities for the Zhou and Ma (2004) study, (a) jet velocity of 0.41 m/s; (b) jet velocity of 11.36 m/s.

changes along the target wall; this aspect is accounted for in the code. The match between experiments and CFD predictions is good (they are within 10%). At the lower velocity, the wall superheat fluctuates quite a lot—hence time-averaged quantities are reported. The results for wall superheat presented here are mesh-independent to within 2%. For both velocities, the fraction of evaporative heat flux is plotted as a function of the applied heat flux. The fraction is simply the heat flux that goes into vaporizing the fluid divided by the total heat flux applied at the wall. As seen in Fig. 8a, at the lower velocity the fraction of evaporative heat flux is quite high – it touches 75% at a flux of 54 W/cm^2. Basically, as the jet velocity is decreased, we move closer to a pool-boiling situation. On the other hand, for the higher velocity case (11.36 m/s), the fraction of evaporative heat flux is only 52% at a heat flux of 250 W/cm^2.

Also, for this higher velocity case, the prediction from a pure single phase case is also shown—i.e. there is no boiling involved. At lower heat fluxes, it can be seen that there is virtually no difference between the single-phase and boiling predictions. However, as the heat flux is increased, the single-phase case shows higher wall temperatures (superheat) as compared to the boiling case—a pointer to the impact of boiling in reducing the wall temperatures.

Overall, these validations give some confidence in the Eulerian multiphase model implemented in FLUENT. Hence, we look at some IGBT package simulations involving boiling jets in the following section.

4. IGBT package simulations with boiling jets

The previous section established some confidence in the CFD predictions of FLUENT by comparing them with experimental data from the literature. This section explores IGBT package simulations with boiling jets.

The axisymmetric domain used in the simulation is shown in Fig. 9. The IGBT package consists of several layers. The silicon die is mounted on a direct bond copper (DBC) stack, which consists of an aluminum nitride layer sandwiched between two copper layers, and the DBC layer is attached to the aluminum baseplate/heat sink. Further details on the IGBT structure can be found in [57]. The boiling simulations are performed on a low resistance IGBT structure as shown in Fig. 9. These boiling simulations are fairly intensive and take several hours to converge on 64-bit Linux machines with 1.4 GHz processor speed—even with a small spatial mesh (i.e., small number of cells).

In the automotive industry, R134a is the working fluid used in the air-conditioning units. Here, we explore the possible use of R134a as the cooling fluid for the IGBTs. The simulations presented here are performed with an R134a (properties given in Table 2) jet inlet temperature of 47 °C. For the boiling simulations, the pressure is maintained at 1.32 MPa (i.e. ~13 atmospheres), at which the saturation temperature of the R134a is 50 °C. So there is a 3 °C sub-cooling in the R134a temperature at the inlet. A volumetric heat generation term is included in the silicon layer to simulate heat dissipation. The results for temperatures are mesh-independent to within 2%. The jet inlet velocity is 2 m/s (Fig. 10a). Fig. 10 shows the contours for velocity, vapor phase fraction, and temperature for the case of 75 W/cm^2 heat dissipation in the silicon die, the jet (diameter = 1.5 mm) velocity is 2 m/s, the jet inlet temperature is 47 °C, with the saturation temperature of 50 °C at a pressure of 1.32 MPa. Table 3 shows two sets of results—one case in which the heat flux dissipation in the silicon die is 75 W/cm^2 with the jet inlet velocity at 2 m/s, while another case in which the heat flux dissipation in the die is 200 W/cm^2 with the jet inlet velocity at 10 m/s. For both cases, jet inlet temperature is 47 °C with a saturation temperature of 50 °C (at 1.32 MPa). Results are quite interesting. At a heat flux of 75 W/cm^2 and 2 m/s

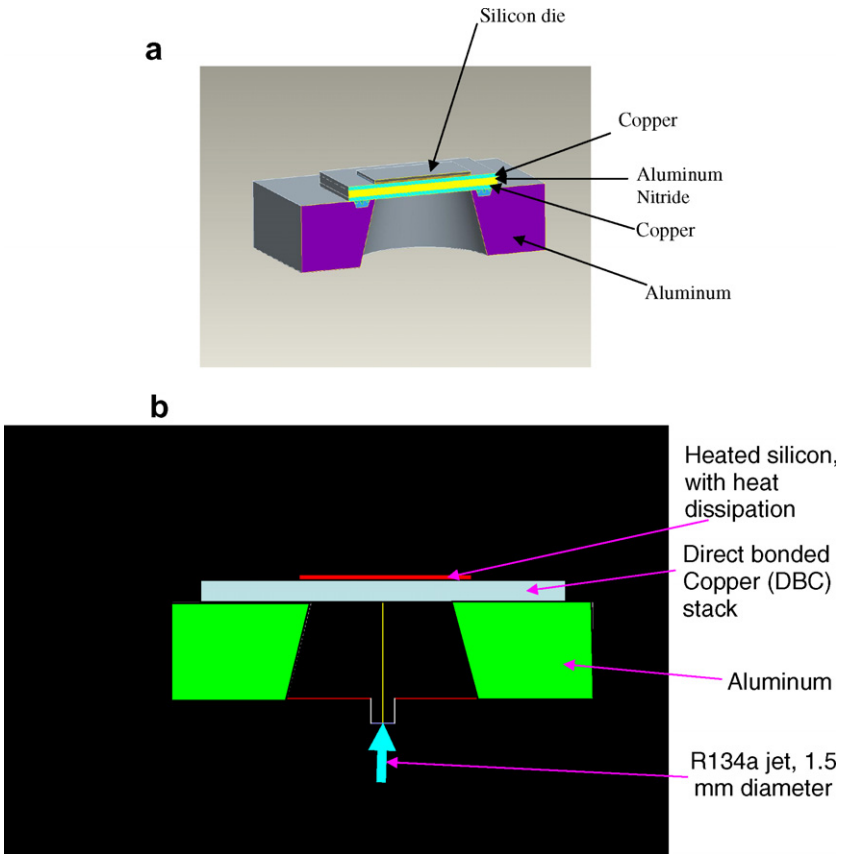

Fig. 9. Axisymmetric domain used for the IGBT package simulation; (a) 3-D view of one IGBT along with the different layers in the package; (b) cross-sectional view of one IGBT and the different layers in the package.

Table 2
Properties of R134a at 1.32 MPa, saturation temperature = 323.15 K

	Liquid	Vapor
Density (kg/m^3)	1103.4	66.16
Specific heat (J/kg K)	1575	1219
Thermal conductivity (W/m K)	0.0735	0.018
Dynamic viscosity (kg/m s)	0.000167	0.0000138

jet velocity, for the case involving boiling, the maximum die temperature is 100.5 °C. For comparison purposes, a case is also shown where the boiling is "switched off" by setting the nucleation site density (Eq. (28)) to zero – which means it becomes a single-phase jet. The temperature when there is no boiling is 115.4 °C. This clearly demonstrates the impact of boiling in reducing the die temperature.

When the heat flux is increased to 200 W/cm^2 and the jet velocity is increased to 10 m/s, for the case involving boiling, the maximum die temperature is 126.3 °C, while for the case when there is no boiling, the maximum temperature is only 110 °C. This is an interesting result—and it suggests that boiling is not beneficial at all jet velocities. The result here suggests that at elevated velocities, boiling may have a detrimental impact upon the heat transfer. Given below is an analysis which clearly shows why this happens.

Eq. (19) can be rewritten as:

$$q''_w = \alpha_l^{cell}[q''_E + q''_Q + q'''_l] + \alpha_v^{cell}[h_{vw} \cdot (T_w - T_v^{cell})] = \alpha_l^{cell}[q''_E + h_l \cdot (T_w - T_l^{cell})] + \alpha_v^{cell}[h_{vw} \cdot (T_w - T_v^{cell})] \quad (35)$$

where liquid phase heat transfer coefficient combines single-phase component and quenching:

$$h_l = h_{lw}(1 - \Omega) + \Omega h_Q \quad (36)$$

Eq. (35) can be solved for wall temperature:

$$T_w = \frac{q''_w}{h_{eff}} + T_{eff} \quad (37)$$

where effective heat transfer coefficient is

$$h_{eff} = \alpha_l^{cell} h_l + \alpha_v^{cell} h_{vw} \quad (38)$$

and effective temperature is

$$T_{eff} = \frac{[(\alpha_l^{cell} h_l T_l^{cell} + \alpha_v^{cell} h_{vw} T_v^{cell}) - \alpha_l^{cell} q''_E]}{h_{eff}} \quad (39)$$

Eqs. (38) and (39) in the single-phase case reduce to ($\alpha_l^{cell} = 1, \alpha_v^{cell} = 0, \Omega = 0, q''_E = 0$):

$$h_{eff} = h_l \quad (40)$$

$$T_{eff} = T_l^{cell} \quad (41)$$

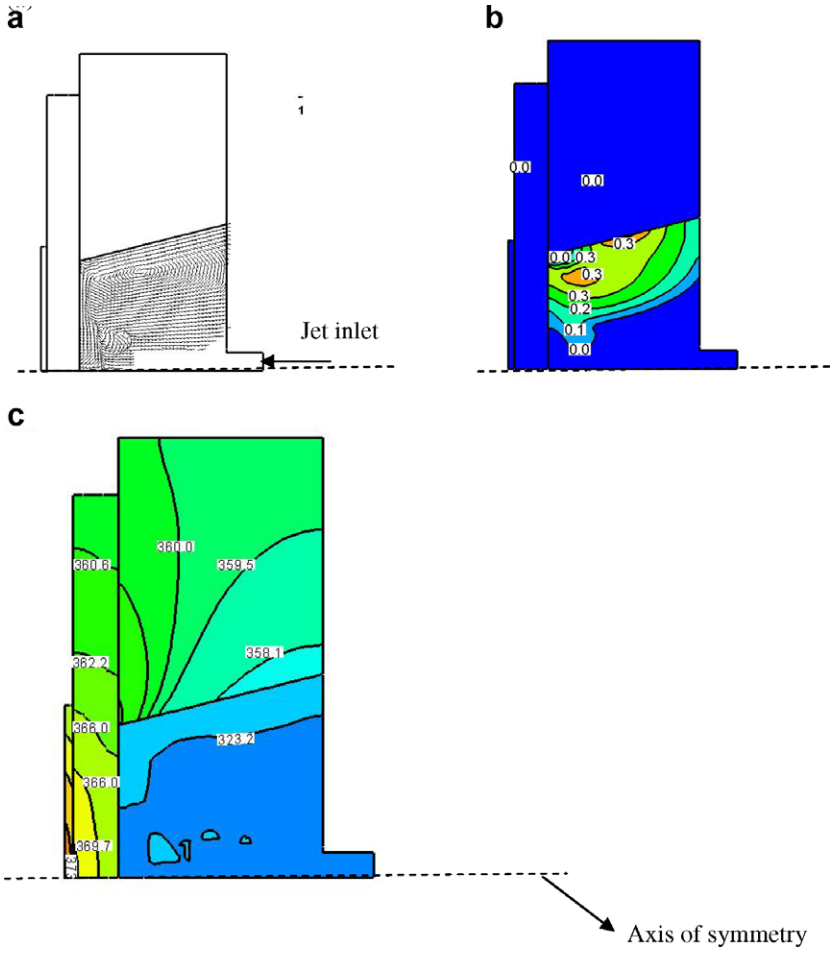

Fig. 10. Representative contours of (a) velocity, (b) vapor fraction, (c) temperature in the domain for 75 W/cm^2, $T_{inlet} = 47$ °C, $T_{sat} = 50$ °C at $P = 1.32$ MPa.

Table 3
Maximum die temperatures for R134a jet (1.5 mm diameter) impingement cooling of the IGBT package involving nucleate boiling, $T_{inlet} = 47$ °C, $T_{sat} = 50$ °C at $P = 1.32$ MPa

	75 W/cm^2, 2 m/s			200 W/cm^2, 10 m/s		
	T_{max} (°C)	h_{Cu} (W/m^2 K)	h_{Al} (W/m^2 K)	T_{max} (°C)	h_{Cu} (W/m^2 K)	h_{Al} (W/m^2 K)
Boiling	100.5	7459	4786	126.3	18,729	9734
No boiling	115.4	6088	3300	110	26476	14,321

For a high jet velocity, $h_{lw} \gg h_Q$, so the appearance of nucleating sites (Ω) can bring down h_l (Eq. (36)), and consequently, h_{eff} (Eq. (38)).

Now comparing Eqs. (39) and (41), one can say that the evaporative part of heat flux q''_E is reducing T_{eff}. So the effect of boiling is to reduce T_{eff}.

So, one can say that at very high convective velocities, the effects of boiling can be detrimental to wall-solid heat transfer. In this case, reduction of T_{eff} by evaporation (Eq. (39)) is offset by decrease in h_{eff} due to the appearance of nucleating sites (Eq. (36)). Actually, degradation of h_{eff} can lead to very high wall superheat and perhaps predict CHF to a certain degree. This may particularly be true when the vapor fraction at the wall is very high. Another observation is that if we neglected heat transfer to the vapor (i.e. $h_{vw} = 0$), then the effect of heat transfer coefficient degradation due to bubbles cannot be captured and boiling would always give lower wall superheat than the no-boiling case. Interestingly, this means that at some velocity in between the two cases we have examined, the boiling and no-boiling cases will yield roughly similar maximum die temperatures.

Table 3 shows the heat transfer coefficients at the aluminum and copper walls. For the low velocity and low flux case (75 W/cm^2 and 2 m/s), the heat transfer coefficients, at the aluminum and copper walls, are higher for the boiling case than for the case which does not involve any boiling. The results are reversed for the high velocity and high

heat flux case (200 W/cm^2 and 10 m/s). Another aspect which should be mentioned is that these results could be dependent on the geometry of the package. For the particular IGBT package geometry considered here, there is a tendency for the vapor to be trapped between the copper and aluminum walls. Since the energy equation for the vapor is being solved, the poor thermal transport properties of the vapor could potentially have a negative impact on the die temperatures.

From a broader FreedomCAR goal perspective, these simulations demonstrate conditions under which R134a can be used to come close to meeting the program goal.

These numerical results need to be validated experimentally. The experimental validations presented in earlier sections give some degree of confidence in the predictions from the code. It would be interesting to see how experimental results from the IGBT package involving boiling would match up with the predictions presented here. Overall, there is evidence of the benefits of boiling from a heat transfer standpoint – though it appears that boiling may not always be beneficial. Although experiments are essential, modeling can yield very useful information when used within their range of applicability. To the best of our knowledge, this is the first time such validations and package simulations are being reported. Tools such as those presented here can be explored for thermal design involving the use of R134a or any other fluid for thermal management in power electronics as well as other electronics cooling applications.

5. Conclusions

The CFD model and code are validated against experimental studies involving submerged jets. To the best of our knowledge, this is the first time such validations are being reported. A reasonable match is found between the experimental boiling curves and those obtained by CFD. IGBT package simulations suggest that, for the case examined here, boiling jets are providing significant benefits over non-boiling jets. However, results suggest that boiling may not necessarily be beneficial in all regimes of jet velocities/heat flux combinations. A tool has been established that can be used for thermal design of two-phase jet impingement cooling systems in the power electronics as well as the broader electronics cooling context.

Acknowledgment

We acknowledge the support and funding provided by Susan Rogers, the program manager for the advanced power electronics and electric machines project under the US Department of Energy FreedomCAR Program.

References

[1] B.W. Webb, C.-F. Ma, Single-phase liquid jet impingement heat transfer, Adv. Heat Transfer 26 (1995) 105–217.
[2] J.H. Lienhard, Liquid jet impingement, Ann. Rev. Heat Transfer (1995) 199–270.
[3] S.V. Garimella, Heat transfer and flow fields in confined jet impingement, Ann. Rev. Heat Transfer (2000) 413–494.
[4] S.V.J. Narumanchi, C.H. Amon, J.Y. Murthy, Influence of pulsating submerged liquid jets on chip-level thermal phenomena, ASME J. Electron. Packaging 125 (2003) 354–361.
[5] Y.Y. Yan, H.B. Zhang, J.B. Hull, Numerical modeling of electrohydrodynamic (EHD) effect on natural convection in an enclosure, Numer. Heat Transfer Part A 46 (2004) 453–471.
[6] T.C. Hung, C.S. Fu, Conjugate heat transfer analysis for the passive enhancement of electronic cooling through geometric modification in a mixed convection domain, Numer. Heat Transfer Part A 35 (1999) 519–535.
[7] L.A. Florio, A. Harnoy, Feasibility study of unconventional cooling of electronic components by vibrating plates at close proximity, Numer. Heat Transfer Part A 47 (2005) 997–1024.
[8] D.H. Wolf, F.P. Incropera, R. Viskanta, Jet impingement boiling, Adv. Heat Transfer 23 (1993) 1–132.
[9] D.W. Zhou, C.F. Ma, Local jet impingement boiling heat transfer with R113, Heat Mass Transfer 40 (2004) 539–549.
[10] I. Mudawar, Assessment of high-heat-flux thermal management schemes, in: International Conference on Thermal, Mechanics and Thermomechanical Phenomena in Electronic Systems, ASME, Las Vegas, NV, 2000, pp. 1–20.
[11] Y. Mitsutake, M. Monde, Ultra high critical heat flux during forced flow boiling heat transfer with an impinging jet, ASME J. Heat Transfer 125 (2003) 1038–1045.
[12] Z.-H. Liu, T.-F. Tong, Y.-H. Qiu, Critical heat flux of steady boiling for subcooled water jet impingement on the flat stagnation zone, ASME J. Heat Transfer 126 (2004) 179–183.
[13] R.J. Copeland, Boiling heat transfer to a water jet impinging on a flat surface (−1g), Ph.D. thesis, Department of Mechanical Engineering, Southern Methodist University, Dallas, TX, 1970.
[14] Y. Katto, M. Kunihiro, Study of the mechanism of burn-out in boiling system of high burn-out heat flux, Bull. JSME 16 (99) (1973) 1357–1366.
[15] Y. Katto, M. Monde, Study of mechanism of burn-out in a high heat-flux boiling system with an impinging jet, in: 5th International Heat Transfer Conference, B6.2, 1974, pp. 245–249.
[16] M. Monde, Y. Katto, Burnout in a high heat-flux boiling system with an impinging jet, Int. J. Heat Mass Transfer 21 (1978) 295–305.
[17] M. Monde, Burnout heat flux in saturated forced convection boiling with an impinging jet, Heat Transfer – Japanese Res. 9 (1) (1980) 31–41.
[18] C.-F. Ma, A.E. Bergles, Boiling jet impingement cooling of simulated microelectronic chips, Heat Transfer in Electronic Equipment, vol. HTD-28, ASME, New York, 1983, pp. 5–12.
[19] C.-F. Ma, A.E. Bergles, Jet impingement nucleate boiling, Int. J. Heat Mass Transfer 29 (8) (1986) 1095–1101.
[20] M.A. Ruch, J.P. Holman, Boiling heat transfer to a Freon-113 jet impinging upward onto a flat, heated surface, Int. J. Heat Mass Transfer 18 (1975) 51–60.
[21] Y. Katto, K. Ishii, Burnout in a high heat flux boiling system with a forced supply of liquid through a plane jet, in: Proceedings of the 6th International Heat Transfer Conference, 1, FB-28, 1978, pp. 435–440.
[22] Y. Miyasaka, S. Inada, Y. Owase, Critical heat flux and subcooled nucleate boiling in transient region between a two-dimensional water jet and a heated surface, J. Chem. Eng. Jpn. 13 (1980) 29–35.
[23] I. Mudawar, D.C. Wadsworth, Critical heat flux from a simulated chip to a confined rectangular impinging jet of dielectric liquid, Int. J. Heat Mass Transfer 34 (6) (1991) 1465–1479.
[24] D.C. Wadsworth, I. Mudawar, Cooling of a multichip electronic module by means of confined two-dimensional jets of dielectric liquid, ASME J. Heat Transfer 112 (1990) 891–898.
[25] T. Nonn, Z. Dagan, L.M. Jiji, Boiling jet impingement cooling of simulated microelectronic heat sources, in: Winter Annual Meeting, ASME, Chicago, Illinois, 88-WA/EEP-3, 1988, pp. 1–9.

[26] T. Nonn, Z. Dagan, L.M. Jiji, Jet impingement flow boiling of a mixture of FC-72 and FC-87 liquids on a simulated electronic chip, in: National Heat Transfer Conference, HTD-vol. 111, 1989, pp. 121–128.
[27] M. Monde, H. Kusuda, H. Uehara, Burnout heat flux in saturated forced convection boiling with two or more impinging jets, Heat Transfer – Japanese Res. (1982) 18–31.
[28] M. Monde, Y. Mitsutake, Critical heat flux in forced convective subcooled boiling with multiple impinging jets, ASME J. Heat Transfer 117 (1996) 241–243.
[29] M.R. Pais, L.C. Chow, E.T. Mahefkey, Multiple jet impingement cooling, J. Thermophys. Heat Transfer 7 (3) (1993) 435–440.
[30] W.M. Rohsenow, A method of correlating heat-transfer data for surface boiling of liquids, Trans. Am. Soc. Mech. Engrs., Paper No. 51-A110, vol. 74, 1952, pp. 969–976.
[31] A. Sharan, J.H. Lienhard, On predicting burnout in the jet-disk configuration, ASME J. Heat Transfer 107 (1985) 398–401.
[32] Y. Katto, S. Yokoya, Critical heat flux on a disk heater cooled by a circular jet of saturated liquid impinging at the center, Int. J. Heat Mass Transfer 31 (2) (1988) 219–227.
[33] M. Monde, Critical heat flux in saturated forced convective boiling on a heated disk with an impinging jet, Warme-und Stoffubertragung 19 (1985) 205–209.
[34] M. Monde, Critical heat flux in saturated forced convection boiling on a heated disk with an impinging jet, ASME J. Heat Transfer 109 (1987) 991–996.
[35] M. Monde, T. Inoue, Critical heat flux in saturated forced convective boiling on a heated disk with multiple impinging jets, ASME J. Heat Transfer 113 (1991) 722–727.
[36] N. Kurul, M.Z. Podowski, Multidimensional effects in forced convection subcooled boiling, in: Ninth International Heat Transfer Conference, Jerusalem, Israel, 1-BO-04., 1990, pp. 21–26.
[37] R.M. Podowski, D.A. Drew, R.T.J. Lahey, M.Z. Podowski, A mechanistic model of the ebullition cycle in forced convection subcooled boiling, in: Eighth International Topical Meeting on Nuclear Reactor Thermal-Hydraulics, Kyoto, Japan, vol. 3, 1997, pp. 1535–1542.
[38] K.O. Pasamehmetoglu, Numerical modeling of a nucleate boiling surface, Numer. Heat Transfer Part A 25 (1994) 703–719.
[39] D. Wang, E. Yu, A. Przekwas, A computational study of two phase jet impingement cooling of an electronic chip, in: Fifteenth IEEE Semi-therm Symposium, IEEE, 1999, pp. 10–15.
[40] N. Seiler, O. Simonin, S. Mimouni, P. Gardin, J.M. Seiler, Modeling and computation of heat exchanges in the configuration of an impinging jet on a hot plate, in: International Conference on Supercomputing in Nuclear Applications, SNA 2003, Paris, France, 2003, pp. 1–13.
[41] A. Mukherjee, V.K. Dhir, Study of lateral merger of vapor bubbles during nucleate pool boiling, ASME J. Heat Transfer 126 (2004) 1023–1039.
[42] X.-Y. Luo, M.-J. Ni, A. Ying, M.A. Abdou, Numerical modeling for multiphase incompressible flow with phase change, Numer. Heat Transfer Part B 48 (2005) 425–444.
[43] D.K. Agarwal, S.W.J. Welch, G. Biswas, F. Durst, Planar simulation of bubble growth in film boiling in near-critical water using a variant of the VOF method, ASME J. Heat Transfer 126 (2004) 329–338.
[44] A. Esmaeeli, G. Tryggvason, Computations of film boiling. Part I: numerical method, Int. J. Heat Mass Transfer 47 (2004) 5451–5461.
[45] A. Esmaeeli, G. Tryggvason, Computations of film boiling. Part II: multi-mode film boiling, Int. J. Heat Mass Transfer 47 (2004) 5463–5476.
[46] K.A. Estes, I. Mudawar, Comparison of two-phase electronic cooling using free jets and sprays, ASME J. Electron. Packaging 117 (1995) 323–332.
[47] L. Lin, R. Ponnappan, Heat transfer characteristics of spray cooling in a closed loop, Int. J. Heat Mass Transfer 46 (2003) 3737–3746.
[48] A.G. Pautsch, T.A. Shedd, Spray impingement cooling with single- and multiple-nozzle arrays. Part I. Heat transfer data using FC-72, Int. J. Heat Mass Transfer 48 (2005) 3167–3175.
[49] F.J. Moraga, F.J. Bonetto, R.T. Lahey, Lateral forces on spheres in turbulent uniform shear flow, Int. J. Multiphase Flow 25 (1999) 1321–1372.
[50] H.C. Unal, Maximum bubble diameter, maximum bubble-growth time and bubble-growth rate during the subcooled nucleate flow boiling of water up to 17.7 M N/m^2, Int. J. Heat Mass Transfer 19 (1976) 643–649.
[51] Y. Wei, C. Morel, Prediction of parameters distribution of upward boiling two-phase flow with two-fluid model, in: Proceedings of ICONE 10, Arlington, VA, USA, 2002, 10pp.
[52] L. Zeng, A unified model for the prediction of bubble detachment diameters in boiling systems – I and II, Int. J. Heat Mass Transfer 35 (9) (1993) 2261–2279.
[53] N. Kolev, The influence of mutual bubble interaction on the bubble departure diameter, Exp. Therm. Fluid Sci. 8 (1994) 167–174.
[54] Koumoutsos, A study of bubble departure in forced-convection boiling, ASME J. Heat Transfer (1968) 223–230.
[55] D.B.R. Kenning, H.T. Victor, Fully-developed nucleate boiling: overlap of areas of influence and interference between bubble sites, Int. J. Heat Mass Transfer 24 (6) (1981) 1025–1032.
[56] A.A. Troshko, Y.A. Hassan, A two-equation turbulence model of turbulent bubbly flows, Int. J. Multiphase Flow 27 (2001) 1965–2000.
[57] S.V.J. Narumanchi, V. Hassani, D. Bharathan, Modeling single phase and boiling liquid jet impingement cooling in power electronics, National Renewable Energy Laboratory, NREL/TP-540-38787, 2005. <http://www.nrel.gov/docs/fy06osti/38787.pdf>.